Build Simul (2016) 9: 281–296
DOI 10.1007/s12273-016-0274-7

Outdoor thermal environment for different urban forms under summer conditions

Yingli Xuan[1] (✉), Guang Yang[2], Qiong Li[3], Akashi Mochida[2]

1. Department of Environmental Engineering and Architecture, Graduate School of Environmental Studies, Nagoya University, Japan
2. Department of Architecture and Building Science, Graduate School of Engineering, Tohoku University, Japan
3. State Key Laboratory of Subtropical Building Science, South China University of Technology, China

Abstract

The present work investigated the outdoor thermal environment for different urban forms under the summer conditions of Sendai, Japan and Guangzhou, China. Sendai has a moderate humid subtropical climate, whereas Guangzhou has a humid subtropical climate. Numerical simulations were performed with a coupled simulation method of convection, radiation, and conduction. A cubic non-linear k–ε model proposed by Craft et al. was selected as the turbulence model and three-dimensional multireflections of shortwave and longwave radiations were considered in the radiation simulation. Seven urban forms (the ratios of building distance to building height were 0.24, 0.36, 0.48, 0.71, 0.95, 1.19, and 1.43.) were studied. The openness and compactness of the urban forms were compared by developing a new assessment system. The following results were obtained. (1) The distributions of wind velocity around the buildings became polarized as building distance decreased, and the proportion of low wind velocity grew large. These conditions mainly caused poor ventilation and thermal discomfort. (2) The cooling effects of building shade became increasingly significant as building distance decreased because of the low level of exposure to strong sunshine in compact forms. (3) Safe outdoor thermal conditions (standard effective temperature ≤37 °C) can be partially achieved in Sendai by decreasing building distance, whereas the same could not be achieved in Guangzhou. Further countermeasures are essential in Guangzhou.

Keywords

urban form,
urban ventilation,
sun–shading,
outdoor thermal environment,
standard effective temperature (SET*)

Article History

Received: 30 January 2015
Revised: 24 October 2015
Accepted: 27 December 2015

1 Introduction

East Asian cities are facing serious environmental problems such as air pollution, large anthropogenic heat release, and urban heat island (UHI) effects (Chan and Yao 2008; Ichinose et al. 1999; Chen et al. 2011; Wang et al. 1990; Oikawa 2011). To reduce the adverse effects of such issues, increasing attention is paid to urban ventilation, especially in coastal cities, by inducing sea breeze to polluted and heated urban areas (Yoshie et al. 2008; Sasaki et al. 2008; Ng 2009; Kato and Hiyama 2012). The successful improvement of urban ventilation greatly depends on the knowledge of wind flow around buildings. Oke (1988) discussed wind flow within building arrays and categorized them into three regimes, namely, isolated roughness flow, wake interference flow, and skimming flow. Kubota et al. (2008a, b) found a strong relationship between mean wind velocity and building density by conducting wind tunnel tests on 27 residential neighborhoods in Japan and Malaysia. Hagishima et al. (2009) investigated the aerodynamic effects of urban-like roughness through wind tunnel experiments, thereby clarifying wind characteristics within and above the urban canopy layer. In addition, the actual wind environment, especially at the pedestrian level (1.5 m above ground level) is considerably complicated and is greatly affected by thermally induced airflow because of the uneven thermal effects of the surroundings. Thermal effects on wind fields must be carefully considered when investigating outdoor wind environment.

As for addressing outdoor thermal comfort, the thermal characteristics of different street canyons (different geometries

E-mail: fighting.xuan@gmail.com

List of symbols

D	building distance (m)	I	turbulence intensity (%)
H	building height (m)	k	turbulence kinetic energy (m^2/s^2)
L	building length (m)	P_k	production term of k (m^2/s^3)
W	building width (m)	T	air temperature (°C)
u	wind velocity in x direction (m/s)	T_{inflow}	air temperature at the inflow boundary (°C)
v	wind velocity in y direction (m/s)	$T_{surface}$	temperature of urban surface (°C)
w	wind velocity in z direction (m/s)	U_s	average wind velocity at the reference height (m/s)
u'	fluctuating velocity component of u (m/s)	Z_G	boundary layer height (m)
v'	fluctuating velocity component of v (m/s)	Z_s	reference height (m)
w'	fluctuating velocity component of w (m/s)	α	power law exponent determined by terrain category (Architectural Institute of Japan 2004)
σ_u	standard deviation of u (m/s)		
σ_v	standard deviation of v (m/s)	α_c	convective heat transfer coefficient ($W/(m^2 \cdot K)$)
σ_w	standard deviation of w (m/s)	ε	energy dissipation rate (m^2/s^3)
C_μ	model constant, 0.09	$\langle\,\rangle$	the symbol for average

and orientations) have been studied (Oke 1988; Arnfield 1990; Spagnolo and de Dear 2003; Bourbia and Awbi 2004; Ali-Toudert and Mayer 2006; Johansson 2006; Johansson and Emmanuel 2006; Hwanga et al. 2011; Yahia and Johansson 2013). This literature review finds the following. (1) At low latitudes, deep street canyons and high building densities are preferable because of the distinct obstruction of solar access at the pedestrian level. (2) North–south oriented street canyons provide more shade than east–west oriented street canyons, except when the sun is at its highest. With the position of the sun during the day, shade appears from the east side of a street to the west side of a street in the former scenario, whereas only the south side is in the shade, and the north side is exposed to the sun in the latter scenario. This condition causes higher mean surface temperatures in the east–west street canyon than in the north–south one for most of the day. The rotation of the street to a northeast–southwest or northwest–southeast orientation is a good compromise as a whole.

At present, studies on urban form have been conducted from the single viewpoint of urban ventilation or sun–shading despite the conflicts between urban forms aimed at providing urban ventilation and sun–shading. The most direct and effective way to improve urban ventilation is to separate buildings, whereas compact forms are favorable for sun–shading. In this study, urban forms are investigated by developing a new assessment system that can evaluate the combined effects of urban ventilation and sun–shading. Moreover, because the intensity of solar radiation at the ground level varies with latitude, the effects of sun–shading and the combined effects of sun–shading and urban ventilation also vary. Sendai (140°52'E, 38°16'N), Japan and Guangzhou (113°33'E, 23°17'N), China are selected as examples to understand the effect of latitude.

Broadly speaking, the relationship between outdoor thermal environment and urban form is affected by (1) climatic conditions, (2) thermal characteristics of urban surfaces (such as moist surfaces, high- or low-albedo surfaces), (3) objects in urban environments (such as trees, overhangs), and (4) the amount of anthropogenic heat release. However, if these factors are taken into account at the same time, it is difficult to understand the contribution of each factor. Therefore, as the first stage of the study, the first factor is selected, and the other factors will be considered one by one in the next stage.

The following three items are discussed in this paper: (1) a new assessment system that can evaluate the combined effects of urban ventilation and sun–shading, (2) comparison of urban forms using the new assessment system under the summer conditions of Sendai and Guangzhou, (3) a predominant factor on outdoor thermal environment under the summer conditions of Sendai and Guangzhou.

2 Analysis outline

2.1 Analysis model

The analysis model in the study is determined by referring to residential areas in Guangzhou, China. Figure 1(a) shows the simplified model of a typical residential area in Guangzhou, China. The buildings (60 m (x) × 15 m (y) × 42 m (z)) are distributed in parallel with each other and face the southeast direction. Owing to the orientation of the buildings, enough sunlight is available in the daytime for indoor spaces, and the advantageous street orientation, that

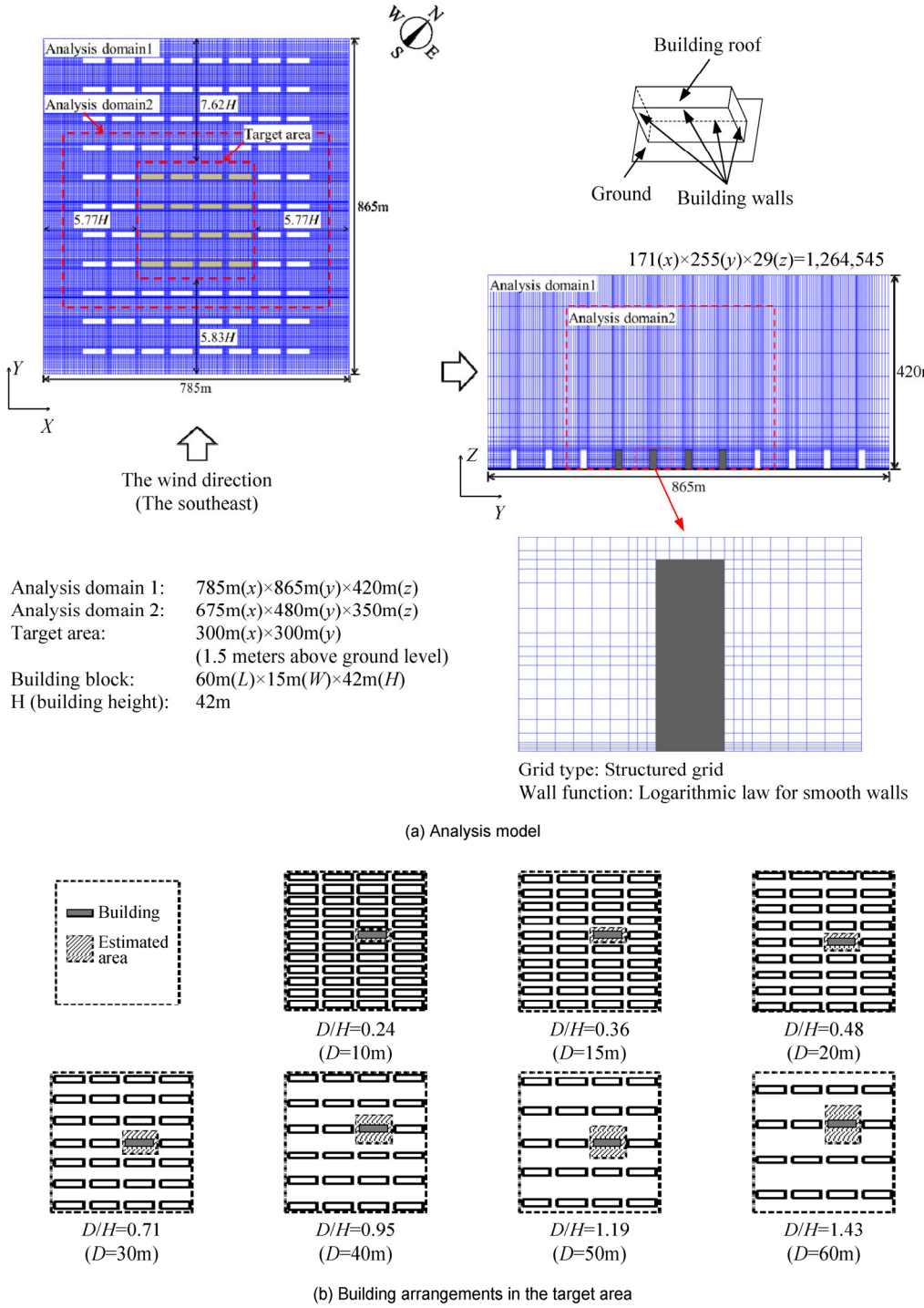

Fig. 1 Analysis model and urban forms in the target area

is, the northeast–southwest orientation, is formed. The main focus area is the target area with a dimension of 300 m (x) × 300 m (y) at 1.5 m above ground level. To ensure the simulation accuracy in the target area, the size of the Analysis domain 1 is determined according to the recommendations in the Architecture Institute of Japan (AIJ) guidelines (Tominaga et al. 2008). The representations of the surroundings play an important role, especially in the simulation of an urban environment. Yoshie et al. (2007) suggested that two or more rows of buildings are required around a target area for practical application. Therefore, the remaining area in this study is built up with a gross building coverage ratio of 16%, which most commonly exists in Sendai, Japan. Although the blockage ratio in this study (6.1%) is greater

than that recommended in the AIJ guidelines (≤3%), the simulation results under such conditions can also be acceptable as long as the blockage ratio is lower than 10% (VDI 2005). In addition, the size and number of meshes also greatly affect simulation accuracy and efficiency. Therefore, a two-stage nested grid technique is used, and the Analysis domain 2 (675 m (x) × 480 m (y) × 350 m (z)) is introduced as a smaller domain with finer meshes compared with the Analysis domain 1.

2.2 Analysis cases

As shown in Fig. 1(b), seven kinds of urban forms in the target area are considered. Building distance changes from 10 m to 60 m while a fixed height of 42 m is given. Provided that urban form can be described by the ratio of building distance (D) to building height (H), D/H, a total of seven values of D/H (0.24, 0.36, 0.48, 0.71, 0.95, 1.19, and 1.43) are investigated under the summer conditions of Sendai and Guangzhou. Table 1 lists all the cases in the study. The case names comprise the city name, building distance, and analysis time. The abbreviations "SD" and "GZ" represent Sendai and Guangzhou, respectively.

2.3 Analysis method

Figure 2 shows the flowchart of the study. It mainly consists of four parts: (1) preparation of input data for boundary conditions; (2) numerical simulations using a coupled simulation method, which includes three-dimensional computational fluid dynamics (CFD) analysis, three-dimensional radiation analysis, and one-dimensional conduction analysis (Yoshida et al. 2000; Chen et al. 2004; Huang et al. 2005; Mochida et al. 2006) (from Steps 1 to 3); (3) evaluation of outdoor thermal comfort by standard effective temperature (SET*) (Gagge et al. 1986) with the simulation results of Step 3 (i.e. wind velocity and air temperature), relative humidity, mean radiant temperature (MRT), and personal variables (Step 4); and (4) comparison of urban forms based on the assessment results of the new assessment system. The coupled simulation method mentioned previously (from Steps 1 to 3) is fulfilled with commercial software STAR-CD V3.26 and STAR-RADX V3.02 with additional codes. STAR-CD is a CFD software package developed by CD adapco Group (2004) that features a finite volume-based flow solver packaged with pre- and post-processors. This software is applicable to most types of flows and provides a high level of accuracy even with complex unstructured meshes. This accuracy can be achieved without sacrificing efficiency. Moreover, the software has the most extensive user subroutine facility and allows numerous actions through its user codes. At present, it is used extensively not only in various industries but also in academia. STAR-RADX is an extended radiation analysis module of STAR-CD. One of the most distinctive features of STAR-RADX is that the absorptivity, reflectivity, and transmissivity properties of an object can be provided at each wavelength band. It also supports specular reflection and radiative heat transfer through transparent objects.

The analysis procedure is described below.

Table 1 Analysis cases

Case name	Analysis date and time	Inflow wind		Building distance D (m)	Building height H (m)	D/H	Gross building coverage ratio in the target area (%)	Floor area ratio in the target area (%)
		Wind velocity (m/s)	Wind direction					
SD-10-12	8/3 12:00	3.6 m/s (at 52.1 m)	The southeast	10	42	0.24	48	672
SD-15-12				15		0.36	40	560
SD-20-12				20		0.48	36	504
SD-30-12				30		0.71	28	392
SD-40-12				40		0.95	24	336
SD-50-12				50		1.19	20	280
SD-60-12				60		1.43	16	224
GZ-10-15	7/14 15:00	2 m/s (at 10 m)	The southeast	10	42	0.24	48	672
GZ-15-15				15		0.36	40	560
GZ-20-15				20		0.48	36	504
GZ-30-15				30		0.71	28	392
GZ-40-15				40		0.95	24	336
GZ-50-15				50		1.19	20	280
GZ-60-15				60		1.43	16	224

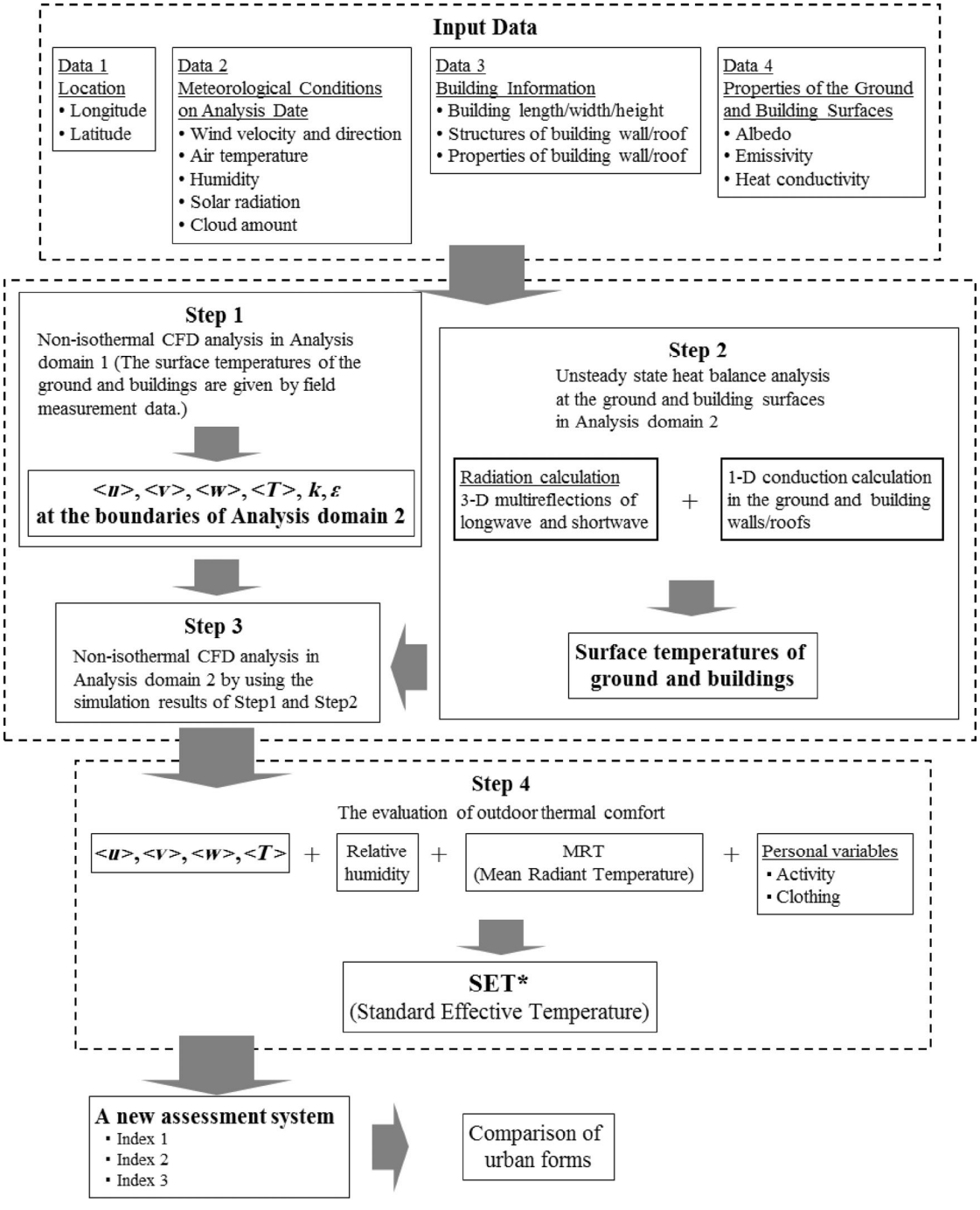

Fig. 2 Flowchart of the study

Step 1: Non-isothermal CFD analysis is carried out in the Analysis domain 1. The purpose of this step is to provide the boundary conditions for Step 3, including three components of wind velocity, air temperature, turbulence kinetic energy, and energy dissipation rate. In this step, the inflow boundary conditions for air temperature and wind velocity are based on the local climatic conditions, and the surface temperatures of the ground and buildings are determined with the field measurement data (Ooyama et al. 2002, Table 4).

Step 2: To obtain the surface temperatures of the ground and buildings, the unsteady-state heat balance analysis of urban surfaces is carried out in the Analysis domain 2. A three-dimensional radiation analysis and a one-dimensional conduction analysis are included in this process.

Step 3: Non-isothermal CFD analysis is carried out in the Analysis domain 2 using the simulation results of Steps

1 and 2 as the boundary conditions. More reliable results can be obtained in this step than in Step 1.

Step 4: Outdoor thermal comfort is evaluated in terms of the SET* (Gagge et al. 1986) in the estimated area (shown in Fig. 1(b)) with the simulation results of Step 3 (i.e. wind velocity and air temperature), relative humidity, MRT, and personal variables (activity and clothing).

2.4 Turbulence model for CFD analysis

In this study, a cubic non-linear k–ε model proposed by Craft et al. (1996) is selected as the turbulence model for the CFD analysis. This turbulence model was originally developed to capture turbulence anisotropy by proposing a cubic relation between stress and strain, which significantly improves the predictions of three-dimensional fluid flow and heat transfer not only in and around a single object (Craft et al. 1996; Suga 2003, 2007) but also around several objects (Raisee et al. 2009). This model has been successfully and widely used in mechanical engineering because of its high prediction accuracy. Its application in the field of wind climate around buildings is tested for the first time by our group. Specifically, its performance is compared with two other turbulence models (the standard k–ε model and the quadratic non-linear k–ε model proposed by Lien et al. (1996)) and shows the best agreement with a wind tunnel experiment from the AIJ benchmark cases (Yoshie et al. 2007; Architectural Institute of Japan 2007). The experimental model and computational conditions are available in the work of Yoshie et al. (2007). Figure 3 shows the correlations of the wind velocity ratios between the CFD simulation results and the wind tunnel experiment results. The gradient of the linear regression line when using the cubic non-linear k–ε model proposed by Craft et al. (1996) is the closest to 1. Hence, this cubic non-linear k–ε model shows the best performance.

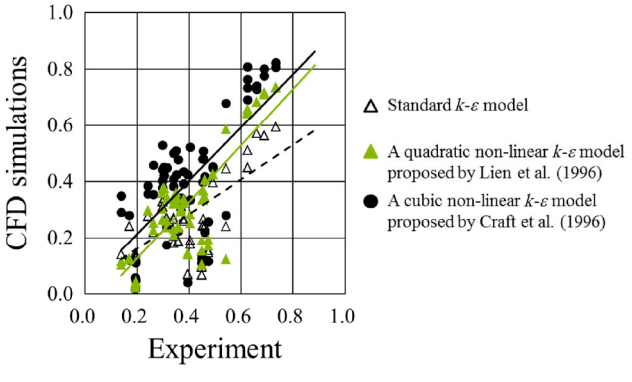

Fig. 3 Correlations of wind velocity ratios between the CFD simulation results and the wind tunnel experiment results

2.5 Heat transfer analysis

To calculate urban surface temperatures, all the surfaces in the computational domain are divided into small surfaces. For each small surface, solar radiation, sky radiation, longwave radiation between it and other surfaces, convective heat transfer and latent heat transfer between it and the ambient air, and conduction heat transfer through it are considered. The shape factor (i.e. configuration factor or view factor) is calculated using the Monte Carlo method (Howell and Perlmutter 1964; Omori et al. 2003), and the radiative heat transfer is calculated using Gebhart's absorption factor (Gebhart 1959). Given that the values of Gebhart's absorption factor are different because of the different absorptivities under shortwave and longwave radiations, they are calculated separately for each surface. According to previous studies (Chen et al. 2004; Huang et al. 2005; Mochida et al. 2006), urban surface temperatures are well reproduced by considering the heat transfers mentioned above.

2.6 Analysis conditions

The analysis date in the study is determined by considering the climatic conditions during the likely occurrence of heat-related illnesses under the summer conditions of Sendai and Guangzhou.

Sendai (140°52'E, 38°16'N), the largest city in the Tohoku region of Japan, has a moderate, humid subtropical climate. Figure 4 shows the monthly averaged daily maximum/mean/minimum temperatures and monthly averaged mean relative humidity in Sendai (1971–2000, source: Japan Meteorological Agency). August is the hottest month (monthly averaged daily maximum temperature, 27.9 °C), and January is the coldest month (monthly averaged daily minimum temperature, −2.0 °C). The mean annual temperature and humidity are 12.1 °C and 70.8%, respectively. According

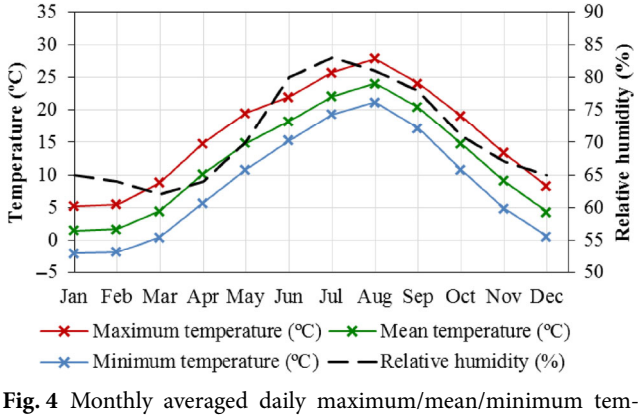

Fig. 4 Monthly averaged daily maximum/mean/minimum temperature and mean relative humidity in Sendai (1971–2000, source: Japan Meteorological Agency)

to the Sendai weather data from the extended automated meteorological data acquisition system (Akasaka et al. 2005), hot weather and hot days over long periods frequently occur in early August, during which people are likely to suffer from heat-related illnesses. Therefore, August 3 is selected as the analysis date for Sendai. The values of the weather parameters during August 3 are determined by averaging the corresponding hourly values in several hot days, which are selected on the basis of the following requirements: (1) the value of the total solar radiation during the whole day at the weather station is greater than 20 MJ/m^2 (hot weather usually occurs in sunny days) and (2) the wind during daytime (from 6:00 a.m. to 6:00 p.m.) blows from the southeast (the prevailing wind direction in summer in Sendai).

However, the climatic conditions in Guangzhou are significantly different from those in Sendai. Guangzhou, the third-largest Chinese city and the largest city in South Central China, is located just south of the Tropic of Cancer and has a humid subtropical climate. Figure 5 shows the monthly averaged daily maximum/mean/minimum temperatures and monthly averaged mean relative humidity in Guangzhou (1971–2000, source: China Meteorological Administration). The summer season, which lasts from May to October, is extremely hot, with a monthly averaged daily maximum temperature of about 30 °C and above, whereas the winter season (December to February) is mild. The mean annual temperature and humidity are 22.6 °C and 77.5%, respectively. People are exposed to the threat of heat-related illnesses throughout the whole summer because of the severe thermal conditions during this period in Guangzhou. Therefore, the analysis date is determined by selecting the day that best represents the average summer conditions (the day in which the diurnal variations of weather parameters are the closest to the average diurnal variations of the corresponding weather parameters throughout the whole summer (Climatic Data Center of China Meteorological Administration, Tsinghua University 2005). Finally, July 14 is selected, and the values of the weather parameters are from the data on that day.

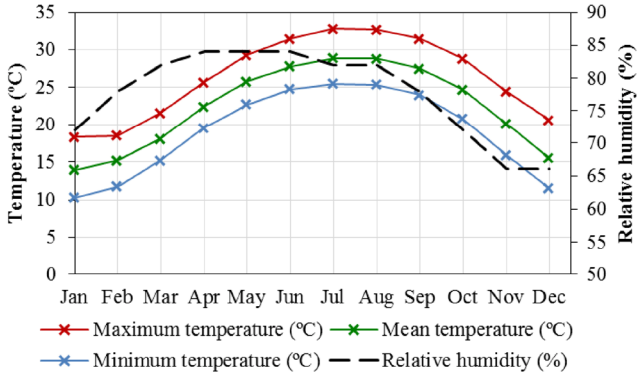

Fig. 5 Monthly averaged daily maximum/mean/minimum temperature and mean relative humidity in Guangzhou (1971–2000, source: China Meteorological Administration)

The analysis time is determined on the basis of the time when the maximum air temperature appears during the analysis date. Thus, 12:00 and 15:00 are selected as the analysis times for Sendai and Guangzhou, respectively, and the air temperatures are 29.3 °C and 32.4 °C, respectively.

The summer prevailing winds in Sendai and Guangzhou are from the southeast. The wind velocities at such direction during the analysis time in Sendai and Guangzhou are 3.6 m/s (at 52.1 m) and 2 m/s (at 10 m), respectively.

A 24 hr unsteady-state heat balance analysis (Step 2) is carried out on the analysis date. Figure 6 shows the structures of the ground and buildings (wall and roof) considered in the heat balance analysis, and Table 2 lists the corresponding thermal properties. The surface properties of the ground and buildings are shown in Table 3. To compare the pure effects of urban form on outdoor thermal environments in Sendai and Guangzhou, the same structures and thermal properties for the buildings in the two cities were given.

The analysis conditions from Steps 1 to 3 are presented in detail in Tables 4, 5, and 6.

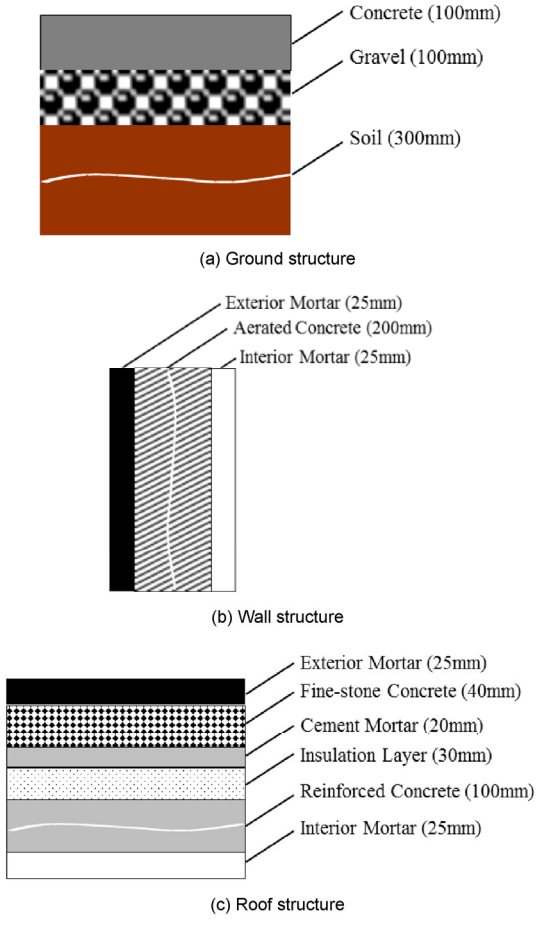

Fig. 6 Structures of the ground and buildings (wall and roof)

Table 2 Structures and thermal properties of ground, wall, and roof

	No. of layers	Material for each layer	Thickness (mm)	Thermal conductivity (W/(m·K))	Specific heat per unit volume (kJ/(m^3·K))
Ground	1	Concrete	100	1.28	1900
	2	Gravel	100	0.62	1500
	3	Soil	300	1.50	3100
Wall	1	Exterior mortar	25	0.93	1890
	2	Aerated concrete	200	0.22	735
	3	Interior mortar	25	0.87	1785
Roof	1	Exterior mortar	25	0.93	1890
	2	Fine-stone concrete	40	1.51	2116
	3	Cement mortar	20	0.93	1890
	4	Insulation layer	30	0.036	41.4
	5	Reinforced concrete	100	1.74	2300
	6	Interior mortar	25	0.87	1785

Table 3 Surface properties of the ground and buildings

	Longwave emissivity	Albedo
Ground (by concrete)	0.90	0.20
Building wall and roof (by mortar)	0.95	0.30

Table 4 Analysis conditions in Step 1

	Sendai	Guangzhou
Analysis date and time	12:00, August 3	15:00, July 14
Domain size (Analysis domain 1)	785 m(x)×865 m(y)×420 m(z)	
Analysis type	Three-dimensional analysis	
Analysis state	Steady state	
Turbulence model	A cubic non-linear k–ε model proposed by Craft et al. (1996)	
Inflow	The wind direction: the southeast $\langle u(z)\rangle = U_s\left(\frac{z}{Z_s}\right)^{\alpha}$ $\alpha = 0.3$ (Architectural Institute of Japan 2004) $Z_s = 52.1$m(Sendai) $= 10$m(Guangzhou) $U_s = 3.6$m/s(Sendai) $= 2$m/s(Guangzhou) $I(z) = \frac{\sigma_u(z)}{\langle u(z)\rangle} = 0.1\left(\frac{z}{Z_G}\right)^{-\alpha-0.05}$, $Z_G = 420$m $k : k(z) = \frac{\sigma_u^2(z)+\sigma_v^2(z)+\sigma_w^2(z)}{2}$ $\cong \sigma_u^2(z)$ $= \left(I(z)\langle u(z)\rangle\right)^2$ $\varepsilon : \varepsilon(z) \cong P_k(z) \cong -\langle u(z)'w(z)'\rangle \frac{\partial\langle u(z)\rangle}{\partial z}$	

Table 4 (continued)

	$\cong C_\mu^{\frac{1}{2}} k(z) \frac{\partial\langle u(z)\rangle}{\partial z}$ $= C_\mu^{\frac{1}{2}} k(z) \frac{U_s}{Z_s} \alpha\left(\frac{z}{Z_s}\right)^{(\alpha-1)}$ $C_\mu = 0.09$ T_{inflow} = 29.3 °C (Sendai) = 32.4 °C (Guangzhou)
Outflow	<u>, <v>, <w>, k, ε, T: zero gradient
Lateral and upper surfaces	<u>, <v>, k, ε: zero gradient <w>=0
Ground and building surfaces	Velocity: Logarithmic law for smooth walls
	Sensible heat flux: α_c =12 W/(m^2·K) Ground surface temperature: 44 °C Building surface temperature: 37 °C
Advection term scheme	<u>, <v>, <w>, k, ε, T: MARS
Coupling algorithm	SIMPLE

Table 5 Analysis conditions in Step 2

	Sendai	Guangzhou
Analysis date and time	August 3 0:00 – August 4 0:00	July 14 0:00 – July 15 0:00
Domain size (Analysis domain 2)	685m (x)×480 m(y)×350 m(z)	
Analysis type	Three-dimensional analysis	
Analysis state	Unsteady state (a 24-hour period)	
Outdoor air temperature	The daily temperature change mode on August 3	The daily temperature change mode on July 14
Indoor air temperature	26°C (an air-conditioning indoor environment is assumed)	
Convective heat transfer coefficient	Outdoor: 12 W/(m^2·K) Indoor: 5 W/(m^2·K)	

Table 6 Analysis conditions in Step 3

	Sendai	Guangzhou
Analysis date and time	12:00, August 3	15:00, July 14
Domain size (Analysis domain 2)	685m(x)×480m(y)×350m(z)	
Analysis type	Three-dimensional analysis	
Analysis state	Steady state	
Turbulence model	A cubic non-linear k–ε model proposed by Craft et al. (1996)	
Inflow boundary, lateral and upper surfaces	<u>, <v>, <w>, k, ε, T: from Step 1	
Outflow	<u>, <v>, <w>, k, ε, T: zero gradient	
Ground and building surfaces	Velocity: Logarithmic law for smooth walls	
	Sensible heat flux: α_c =12 W/(m^2·K) $T_{surface}$: from Step 2	
Advection term scheme	<u>, <v>, <w>, k, ε, T: MARS	
Coupling algorithm	SIMPLE	

3 Assessment outline

At present, the most commonly used thermal comfort indices are based on the heat budget of the human body; examples include the predicted mean vote (PMV; Fanger 1972), SET* (Gagge et al. 1986), physiologically equivalent temperature (PET; Höppe 1999), and universal thermal climate index (UTCI). The PMV index proposed by Fanger (1972) is the first thermal comfort index based on the heat budget of the human body. This index is based on Fanger's one-node model and was originally conceived for indoor conditions. The UTCI is a state-of-the-art thermal comfort index for outdoor applications. It is based on one of the most advanced multi-node thermophysiological models (Fiala et al. 1999, 2001, 2003) and is integrated with an adaptive clothing model developed by Richards and Havenith (2007). Although all the mechanisms of heat exchange can be universally valid and applicable to all climates, seasons, and scales, some adjustments are still necessary for local applications because of the differences in the thermal sensation of people at different places. De Dear and Spagnolo (2002) argued that regional calibration should be carried out using local subjective thermal comfort data. Accordingly, the UTCI is not considered in the present work because of the lack of studies for Sendai and Guangzhou. The basis of the SET* index is Gagge's two-node model (Gagge et al. 1971), whereas that of the PET index is the Munich energy balance model for individuals (Höppe 1999). The SET* index has a solid basis for indoor applications, whereas the PET index is primarily designed for outdoor applications. However, the SET* index can also be applicable to outdoor conditions by using outdoor environmental variables (e.g. OUT_SET* (Pickup and de Dear 2000)). The most distinct difference between the SET* and the PET is the way in which physiological sweat rate is calculated. Sasaki et al. (2009) compared the sensitivity of relative humidity in these two indices and recommended that the SET* is more suitable than the PET in assessing hot and humid environments in Asian cities. Finally, the SET* is selected in this study to evaluate the outdoor thermal environment in Sendai and Guangzhou. The method used to calculate SET* has been developed by Yoshida et al. (2000).

The SET* is an indicator that facilitates the overall evaluation of thermal comfort with consideration of the effects of (1) wind velocity, (2) air temperature, (3) relative humidity, (4) MRT, (5) clothing, and (6) metabolism. In the calculation of the SET*, outdoor environmental variables (i.e. wind velocity, air temperature, relative humidity, and MRT) are used. The first two parameters are obtained with a numerical simulation using the coupled simulation method mentioned previously (Step 3). The third parameter, that is, relative humidity, is calculated by establishing a uniform spatial distribution of absolute humidity and converting it to relative humidity at a given temperature (the spatial distributions of air temperature are determined from Step 3)[Note 1)]. The fourth parameter, that is, MRT, is calculated by using the method proposed by Nakamura (1987)[Note 2)]. The way people dress and perform activities is unique in every city. Therefore, the appropriate clothing and activity values differ with location. However, no appropriate values for clothing and activity levels are currently available for Sendai and Guangzhou. Moreover, to purely compare the combined effects of outdoor environmental variables on outdoor thermal conditions at different locations, the same clothing and activity levels must be used. Accordingly, the amount of clothing and the metabolism of the human body are assumed to be 0.6 clo (briefs, 0.05 clo; short sleeve shirt, 0.22 clo; trousers, 0.26 clo; socks, 0.03 clo; shoes, 0.04 clo (Butera 1998)) and 1.4 met, which correspond to the thermal insulation of summer clothing and the intermediate state of standing relaxed (1.2 met) and standing with light-intensity activities (1.6 met) (Fanger 1972), respectively.

In general, the upper limit of the SET* varies by location because of climatic conditions and the thermal adaptation of people. A large number of studies are required to determine the above value in each location. Unfortunately, no data are currently available for Sendai or Guangzhou. The study by Blazejczyk et al. (2012) indicated that when the SET* exceeds 37 °C, the outdoor thermal environment becomes too dangerous for people. Accordingly, the upper limit of the SET* in this study is considered to be 37 °C for both Sendai and Guangzhou. A new assessment system is developed by focusing on safe outdoor thermal conditions in summer (the values of SET* are lower than the upper limit, 37 °C; Blazejczyk et al. 2012). The openness and compactness of urban form are compared with the following three assessment approaches.

3.1 Assessment approach 1

The essential point of this assessment is to examine urban form in terms of the area where the value of the SET* is less than 37 °C (= Index 1). However, one limitation is that the comparison of urban forms with Index 1 is reasonable only when planned areas are the same.

3.2 Assessment approach 2

To enable the comparison of urban forms regardless of planned area, assessment approach 2 is introduced by dividing

Index 1 by the planned area (= Index 2). This approach can be described as follows:

$$\text{Index 2} = \frac{A_{\text{SET}^*\leq 37^\circ\text{C}}}{A_{\text{planned}}} \times 100\% \quad (1)$$

where

$A_{\text{SET}^*\leq 37^\circ\text{C}}$: area where the value of the SET* is less than 37 °C (m²);

$A_{\text{planned area}} = A_{\text{open space}} + A_{\text{building}}$;

$A_{\text{open space}}$: open space in the planned area (m²);

A_{building} : building area in the planned area (m²).

However, when the same assessment results are obtained with Index 2 under different urban forms, the comparison becomes difficult. The introduction of the following assessment approach is necessary.

3.3 Assessment approach 3

Assessment approach 3 is introduced by dividing Index 1 by the open space (= Index 3), as shown in Eq. (2).

$$\text{Index 3} = \frac{A_{\text{SET}^*\leq 37^\circ\text{C}}}{A_{\text{open space}}} \times 100\% \quad (2)$$

Index 3 indicates the percentage of open spaces with safe outdoor thermal conditions (SET* ≤ 37 °C; Blazejczyk et al. 2012). Thus, a high Index 3 value equates to a safe outdoor thermal environment.

Overall, high Index 2 and Index 3 values equate to a good urban form.

4 Results and discussion

4.1 Wind velocity

Figure 7 shows the distributions of the pedestrian level wind velocity (at 1.5 m) in Sendai and Guangzhou. According to the distributions of wind velocity in the *XY* plane at 1.5 m, relatively high wind velocities in the wind paths parallel to the incoming wind direction and relatively low wind velocities in the wind paths perpendicular to the incoming wind direction are observed when building distance (*D*) is 10 m. This result can be explained as follows. (1) With regard to the incoming wind within the building height, only a small amount of it blows into the narrow street perpendicular to the incoming wind direction, and most of it passes straight through the wind paths parallel to the incoming wind direction. (2) The incoming wind over buildings cannot enter the spaces between buildings. Accordingly, it will not

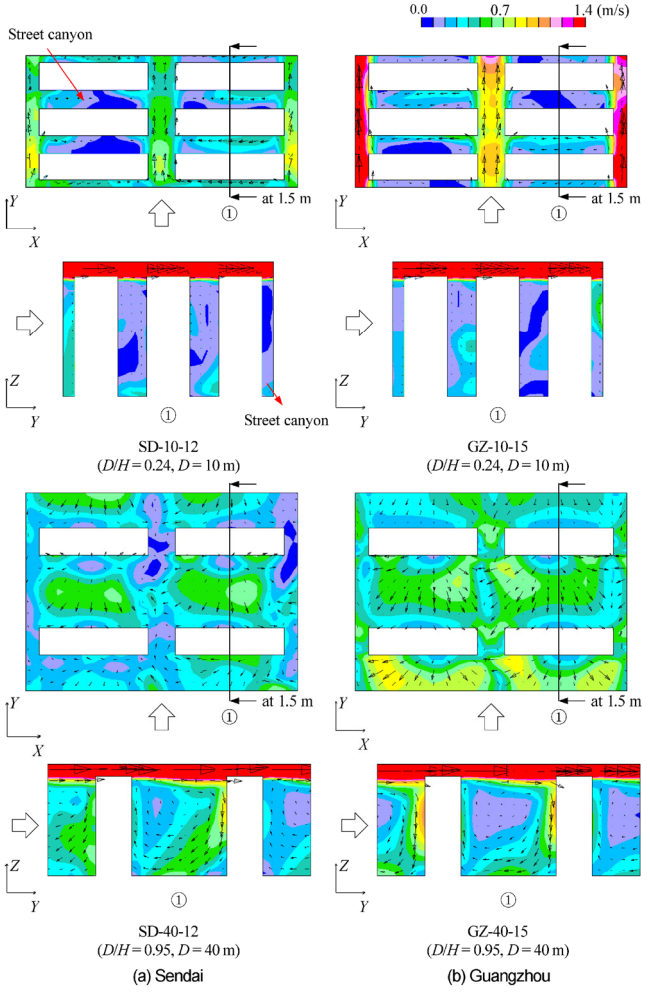

Fig. 7 Distributions of the pedestrian level wind velocity (at 1.5 m) in Sendai (at 12:00) and Guangzhou (at 15:00)

affect the pedestrian level wind environment (refer to the distributions of wind velocity in the *YZ* plane when *D* is 10 m in Fig. 7). However, when *D* is 40 m, the incoming wind over buildings plays an important role. A recirculating flow is formed between buildings (refer to the distributions of wind velocity in the *YZ* plane when *D* is 40 m in Fig. 7), and it directly affects the distributions of the pedestrian level wind velocity (refer to the distributions of wind velocity in the *XY* plane when *D* is 40 m in Fig. 7). Therefore, the pedestrian level wind velocity is evenly distributed.

The above findings can also be observed in Fig. 8, which summarizes the probability density of the pedestrian level wind velocity (at 1.5 m) in each urban form in Sendai and Guangzhou. The figure illustrates that the wind velocity distributions around the buildings become polarized as building distance decreases, and an increase in the proportion of low wind velocity will cause poor ventilation and thermal discomfort (Murakami and Morikawa 1985). These findings suggest that building distance cannot be reduced excessively.

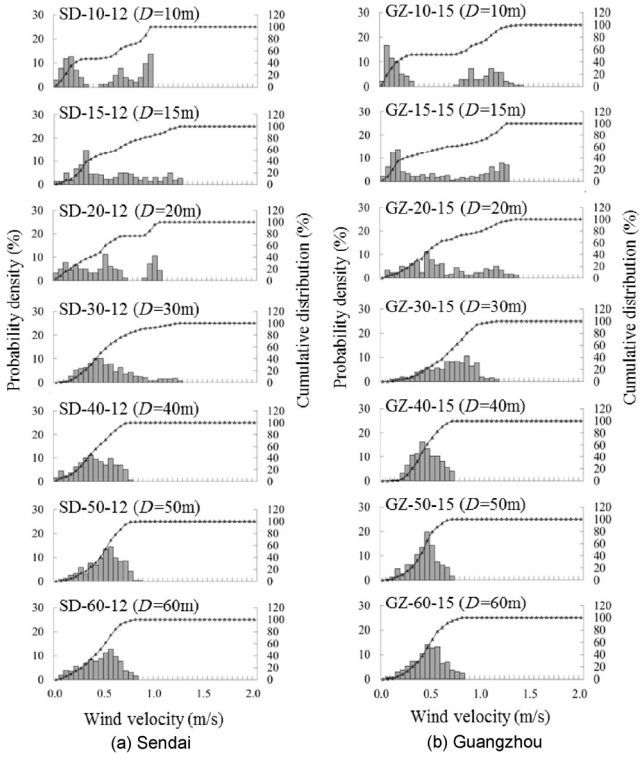

Fig. 8 Probability density and cumulative distribution of the pedestrian level wind velocity (at 1.5 m) in the estimated area in Sendai (at 12:00) and Guangzhou (at 15:00)

4.2 Surface temperature, MRT, and SVF

Figure 9 shows the distributions of surface temperature in Sendai and Guangzhou. A small reduction in surface temperature occurs when building distance decreases from 60 m to 30 m. However, surface temperature falls sharply when building distance further decreases from 30 m to 10 m. This effect is related to the interrelationships between buildings. The shadow of each building is isolated when buildings are widely separated, whereas in compact forms, buildings are close enough to provide shade to nearby buildings. A similar tendency can also be seen in the MRT shown in Figs. 10 and 11. These findings are closely related to the change tendency of the sky view factor (SVF [Note 3)], shown in Fig. 12) with a decrease in building distance. Because the SVF which denotes the ratio of radiation received by a planar surface to that from the entire hemispheric radiating environment plays a decisive role on surface temperature and MRT. Thus, outdoor thermal environment can be improved by reducing building distance.

4.3 SET* and the assessment results of the new assessment system

Figure 13 shows the distributions of the SET* at the pedestrian level (at 1.5 m) in Sendai and Guangzhou. The outdoor

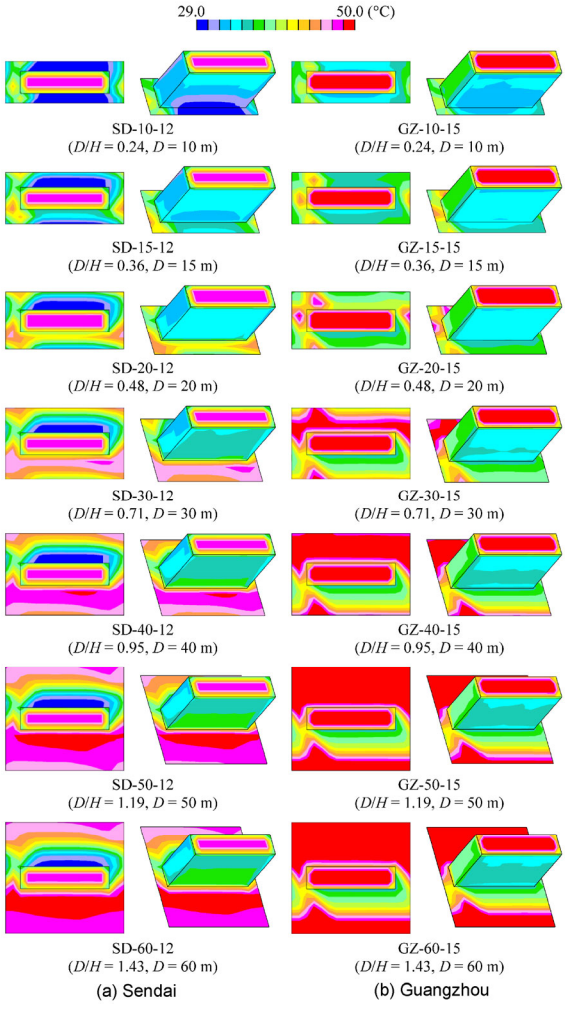

Fig. 9 Distributions of surface temperature in the estimated area in Sendai (at 12:00) and Guangzhou (at 15:00)

thermal environment becomes increasingly comfortable as building distance decreases. Table 7 summarizes the average SET* at the pedestrian level (at 1.5 m) in Sendai and Guangzhou. The average SET* decreases gradually as building distance decreases, mainly because of the cooling effects of building shade resulting from reduced building distance (Figs. 9, 10, 11 and 12).

Figure 14 shows the probability density and cumulative distribution of the SET* at the pedestrian level (at 1.5 m) in Sendai and Guangzhou. According to Fig. 14(a), no area is safe (SET* ≤ 37 °C) when building distances are 40, 50, and 60 m. This condition is affected by the level of exposure to strong sunshine, as indicated by a high SVF (shown in Fig. 12) and high MRT (shown in Fig. 11). With a decrease in building distance from 30 m to 10 m, the cooling effects of building shade become increasingly effective, and the safe area (SET* ≤ 37 °C) gradually increases, except when building distance is 15 m. This condition is caused by the combined effects of building shade and wind velocity. When

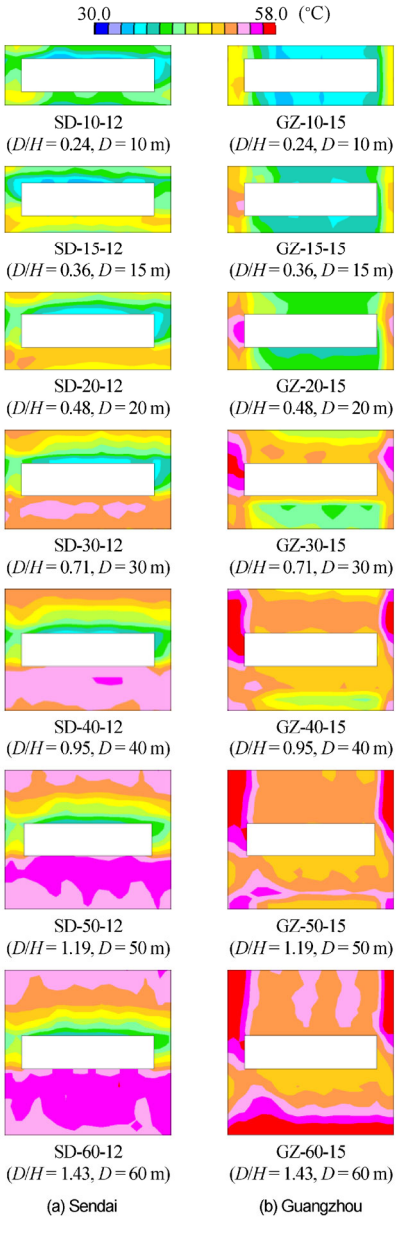

Fig. 10 Distributions of MRT at the pedestrian level (at 1.5 m) in the estimated area in Sendai (at 12:00) and Guangzhou (at 15:00)

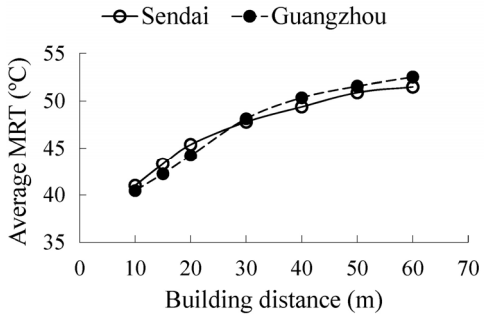

Fig. 11 Average MRT at the pedestrian level (at 1.5 m) in the estimated area in Sendai (at 12:00) and Guangzhou (at 15:00)

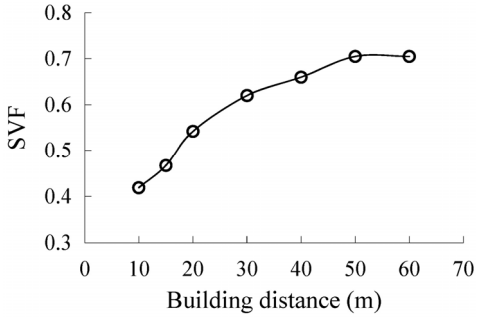

Fig. 12 Relationship between building distance and SVF

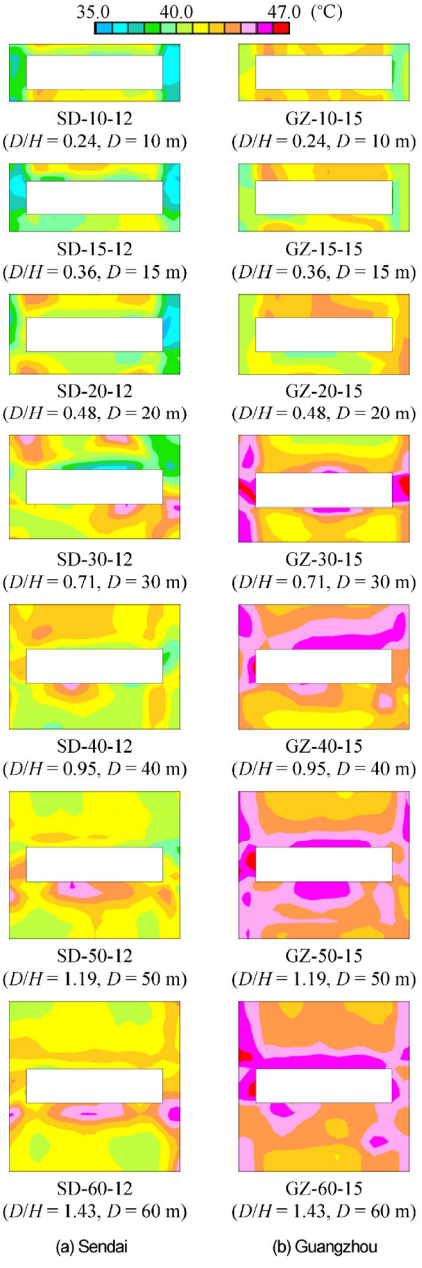

Fig. 13 Distributions of SET* at the pedestrian level (at 1.5 m) in the estimated area in Sendai (at 12:00) and Guangzhou (at 15:00)

Table 7 Average SET* and assessment results with Indices 1, 2, and 3 in the estimated area at 1.5 m

Case name	Average SET* (°C)	Index 1 in the estimated area (m^2)	Index 2 in the estimated area (%)	Index 3 in the estimated area (%)
SD-10-12	39.0	229.4	0.12	23.5
SD-15-12	39.8	95.6	0.04	7.1
SD-20-12	39.9	230.0	0.09	13.3
SD-30-12	40.9	87.5	0.03	3.5
SD-40-12	41.2	0.0	0.0	0.0
SD-50-12	41.3	0.0	0.0	0.0
SD-60-12	41.8	0.0	0.0	0.0
GZ-10-15	41.1	0.0	0.0	0.0
GZ-15-15	41.1	0.0	0.0	0.0
GZ-20-15	41.5	0.0	0.0	0.0
GZ-30-15	42.5	0.0	0.0	0.0
GZ-40-15	43.4	0.0	0.0	0.0
GZ-50-15	43.7	0.0	0.0	0.0
GZ-60-15	43.8	0.0	0.0	0.0

building distance is 20 m, the cooling effects of building shade are less effective than those in the case when building distance is 15 m (shown in Figs. 9, 10, 11, and 12). However, the thermal discomfort caused by low wind velocity is highly significant when building distance is 15 m and overcomes the cooling effects of building shade. Therefore, only a few safe areas (SET* ≤ 37 °C) appear when building distance is 15 m. The relationship between the cooling effects of building shade and the thermal discomfort caused by low wind velocity is reversed when building distance is 10 m. That is, the cooling effects of building shade become overwhelmingly high, and although the thermal discomfort caused by low wind velocity increases, the combined effects of building shade and wind velocity are positive. Accordingly, only a few safe areas (SET* ≤ 37 °C) appear when building distance is 15 m.

As shown in Fig. 14(b), no safe area (SET* ≤ 37 °C) forms in all cases in Guangzhou. As seen from Figs. 8 and 11, the wind velocity and MRT in Sendai and Guangzhou do not significantly differ. The difference in the amount of safe area (SET* ≤ 37 °C) between Sendai and Guangzhou is most likely because of air temperature. As shown in Table 4, the air temperature at the inflow boundary in Guangzhou is 3.1 °C higher than that in Sendai.

According to the assessment results of the new assessment system shown in Table 7, safe outdoor thermal conditions can be partially achieved in Sendai by decreasing building distance, whereas the same could not be achieved in Guangzhou because of its severe climatic conditions in summer. Further countermeasures are thus essential in Guangzhou.

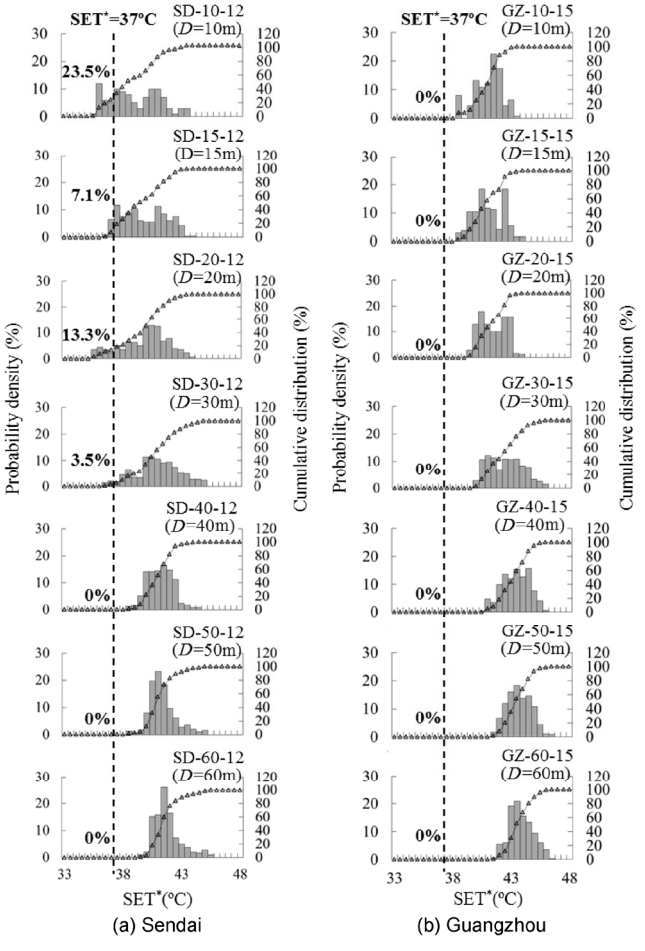

Fig. 14 Probability density and cumulative distribution of SET* at the pedestrian level (at 1.5 m) in the estimated area in Sendai (at 12:00) and Guangzhou (at 15:00)

5 Conclusions

In this paper, the following three points are highlighted.

(1) A new assessment system is developed with the capability of evaluating the combined effects of urban ventilation and sun–shading. Given that the system is combined with the upper limit of the SET*, assessing the actual outdoor environment and applying the system to real projects are possible if the specific SET* value at any place is available.

(2) Safe outdoor thermal conditions can be partially achieved in Sendai by decreasing building distance, whereas the same could not be achieved in Guangzhou because of its severe climatic conditions in summer. Further countermeasures are essential in Guangzhou.

(3) The MRT is the predominant factor that determines the outdoor thermal environment under certain climatic conditions at which heat-related illnesses are likely to occur in Sendai and Guangzhou. This result indicates that

the outdoor thermal environment can be significantly improved by reducing building distance. However, building distance cannot be reduced excessively because the large proportion of low wind velocity causes poor ventilation and thermal discomfort.

Acknowledgements

The authors would like to thank the Strategic Japanese–Chinese Cooperation Program of JST and MOST (Grant no. 2011DFA91210) for their financial support.

Notes

Note 1): In this study, the surfaces of the ground and buildings are covered with concrete and mortar (shown in Fig. 6 and Table 2), and no other moisture sources exist in the whole area. Therefore, solving the transport equation of moisture is unnecessary. Finally, relative humidity is calculated with the constant value of absolute humidity (0.024 kg/kg′), which is determined from the climatic conditions of Guangzhou, China at 15:00 on July 14.

Note 2): In this study, the MRT is calculated using the method proposed by Nakamura (1987). In the method of Nakamura (1987), the human body is approximated to a rectangular prism (shown in Fig. N1), and the amount of radiant heat absorbed by the human body is estimated with the weighting factor for the radiant heat flux from each direction. Equation (N1) shows the calculation of the MRT.

$$\sigma T_{\mathrm{mrt}}^4 = \sum_{l=-3}^{3} q_l \alpha_{\mathrm{h}} c_l + \sum_{l=-3}^{3} \left(\sum_{j=1}^{n} B_{lj} \sigma T_j^4 c_l \right) \quad \text{(N1)}$$

where

T_{mrt}: mean radiant temperature (MRT) (K)

l: surface index of a rectangular prismatic human body, $l = -3 - +3$

q_l: amount of shortwave radiation (direct, sky, and diffuse solar radiation) at surface l of a rectangular prismatic human body (W/m^2)

α_{h}: shortwave radiation absorption coefficient for human body, $\alpha_{\mathrm{h}} = 0.5$

c_l: weighting factor for surface l of a rectangular prismatic human body, for the top and bottom surfaces, 0.024; for the lateral surfaces, 0.238

T_j: temperatures of the surfaces surrounding a rectangular prismatic human body (K)

B_{lj}: Gebhart absorption coefficient from surface l of a rectangular prismatic human body to surface j

σ Stefan–Boltzmann constant, 5.67×10^{-8} W/(m^2·K^4)

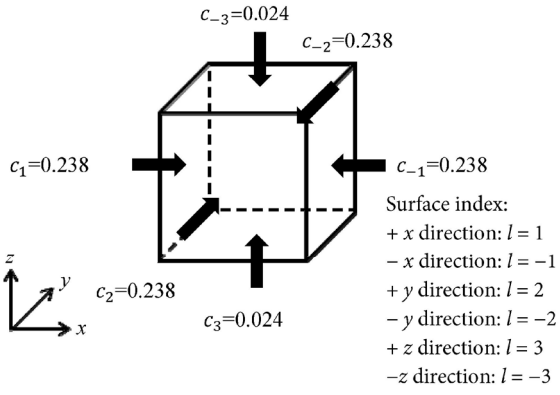

Fig. N1 A rectangular prismatic human body

Note 3): In this study, the SVF is calculated by simplifying the method proposed by Li et al. (2006), and the algorithm is fulfilled with software DUTE 1.0 (Design Tool for Urban Residential Area Thermal Environment, Registration number: 2008SR12279, South China University of Technology 2008).

References

Akasaka H, et al. (2005). Extended AMeDAS Weather DATA 1981–2000. Kagoshima Technology Licensing Organization. (in Japanese)

Ali-Toudert F, Mayer H (2006). Numerical study on the effects of aspect ratio and orientation of an urban street canyon on outdoor thermal comfort in hot and dry climate. *Building and Environment*, 41: 94–108.

Architectural Institute of Japan (2004). Recommendations on Loads for Buildings. (in Japanese)

Architectural Institute of Japan (2007). Guidebook for practical applications of CFD to pedestrian wind environment around buildings. Available at http://www.aij.or.jp/jpn/publish/cfdguide/index_e.htm.

Arnfield AJ (1990). Street design and urban canyon solar access. *Energy and Buildings*, 14: 117–131.

Blazejczyk K, Epstein Y, Jendritzky G, Staiger H, Tinz B (2012). Comparison of UTCI to selected thermal indices. *International Journal of Biometeorology*, 56: 515–535.

Butera FM (1998). Chapter 3—Principles of thermal comfort. *Renewable and Sustainable Energy Reviews*, 2: 39–66.

Bourbia F, Awbi HB (2004). Building cluster and shading in urban canyon for hot dry climate: Part 2: Shading simulations. *Renewable Energy*, 29: 291–301.

CD adapco Group (2004). Chapter 6: Turbulent flow boundary conditions. In: STAR-CD Version 3.2 Methodology.

Chan CK, Yao X (2008). Air pollution in mega cities in China—A review. *Atmospheric Environment*, 42: 1–42.

Chen B, Shi G, Dai T, Shen Y, Wang B, Yang S, Zhao J (2011). Climate forcing due to anthropogenic heat release over China. *Climatic and Environmental Research*, 16: 717–722. (in Chinese)

Chen H, Ooka R, Harayama K, Kato S, Li X (2004). Study on outdoor thermal environment of apartment block in Shenzhen, China with coupled simulation of convection, radiation and conduction. *Energy and Buildings*, 36: 1247–1258.

Climatic Data Center of China Meteorological Administration, Tsinghua University (2005). Meteorological Data Set for China Building Thermal Environment Analysis. Beijing: China Architecture and Building Press. (in Chinese)

Craft TJ, Launder BE, Suga K (1996). Development and application of a cubic eddy-viscosity model of turbulence. *International Journal of Heat and Fluid Flow*, 17: 108–115.

Fanger PO (1972). Thermal Comfort. New York: McGraw-Hill.

de Dear RJ, Spagnolo JC (2002). Thermal comfort outdoors. In: Proceedings of 10th International Conference on Environmental Ergonomics (ICEE), Fukuoka, Japan.

Fiala D, Lomas KJ, Stohrer M (1999). A computer model of human thermoregulation for a wide range of environmental conditions: The passive system. *Journal of Applied Physiology*, 87: 1957–1972.

Fiala D, Lomas KJ, Stohrer M (2001). Computer prediction of human thermoregulatory and temperature responses to a wide range of environmental conditions. *International Journal of Biometeorology*, 45: 143–159.

Fiala D, Lomas KJ, Stohrer M (2003). First principles modelling of thermal sensation responses in steady state and transient boundary conditions. *ASHRAE Transactions*, 109(1): 179–186.

Gagge AP, Stolwijk JAJ, Nishi Y (1971). An effective temperature scale based on a simple model of human physiological regulatory response. *ASHRAE Transactions*, 77(1): 247–262.

Gagge AP, Fobelets AP, Berglund PE (1986). A standard predictive index of human response to the thermal environment. *ASHRAE Transactions*, 92(2): 709–731.

Gebhart B (1959). A new method for calculating radiant exchanges. *ASHRAE Transactions*, 65(1): 321–332.

Hagishima A, Tanimoto J, Nagayama K, Meno S (2009). Aerodynamic parameters of regular arrays of rectangular blocks with various geometries. *Boundary-Layer Meteorology*, 132: 315–337.

Hardy JD (1970). Thermal comfort and health. Paper presented at 2nd Human Factors Symposium, ASHRAE Semiannual Meeting, San Francisco, USA.

Höppe P (1999). The physiological equivalent temperature—A universal index for the biometeorological assessment of the thermal environment. *International Journal of Biometeorology*, 43: 71–75.

Howell JR, Perlmutter M (1964). Monte Carlo solution of thermal transfer through radiant media between gray walls. *Journal of Heat Transfer*, 86: 116–122.

Huang H, Ooka R, Kato S (2005). Urban thermal environment measurements and numerical simulation for an actual complex urban area covering a large district heating and cooling system in summer. *Atmospheric Environment*, 39: 6362–6375.

Hwanga R-L, Lin T-P, Matzarakis A (2011). Seasonal effects of urban street shading on long-term outdoor thermal comfort. *Building and Environment*, 46: 863–870.

Ichinose T, Shimodozono K, Hanaki K (1999). Impact of anthropogenic heat on urban climate in Tokyo. *Atmospheric Environment*, 33: 3897–3909.

Johansson E (2006). Influence of urban geometry on outdoor thermal comfort in a hot dry climate: A study in Fez, Morocco. *Building and Environment*, 41: 1326–1338.

Johansson E, Emmanuel R (2006). The influence of urban design on outdoor thermal comfort in the hot, humid city of Colombo, Sri Lanka. *International Journal of Biometeorology*, 51: 119–133.

Kato S, Hiyama K (2012). Ventilating Cities—Air-flow Criteria for Healthy and Comfortable Urban Living. Heidelberg: Springer.

Kubota T, Miura M, Ahmad S, Tominaga Y, Mochida A (2008a). Planning methods of residential neighborhoods for achieving acceptable wind environment under local climate conditions: A comparison of Japanese and Malaysian cases. In: Proceedings of 4th International Conference on Advances in Wind and Structures, Jeju, Korea, pp.1608–1616.

Kubota T, Miura M, Tominaga Y, Mochida A (2008b). Wind tunnel tests on the relationship between building density and pedestrian-level wind velocity: Development of guidelines for realizing acceptable wind environment in residential neighborhoods. *Building and Environment*, 43: 1699–1708.

Li BZ, Luo Q, Yao RM (2006). Solution on configuration factor from ground to sky. *Journal of Chongqing University (Natural Science Edition)*, 29(2): 86–89. (in Chinese)

Lien FS, Chen WL, Leschziner MA (1996). Low-Reynolds-number eddy-viscosity modeling based on non-linear stress–strain/vorticity relations. In: Proceedings of 3rd Symposium on Engineering Turbulence Modeling and Measurement, Heraklion crete, Greece.

Mochida A, Yoshino H, Miyauchi S, Mitamura T (2006). Total analysis of cooling effects of cross-ventilation affected by microclimate around a building. *Solar Energy*, 80: 371–382.

Murakami S, Morikawa Y (1985). Criteria for assessing wind-induced discomfort considering temperature effect. *Transactions of AIJ, Journal of Architecture and Planning*, 358: 9–17. (in Japanese)

Nakamura Y (1987). Expression method of the radiant filed on a human body in buildings and urban space. *Transactions of AIJ, Journal of Architecture and Planning*, 376: 29–35. (in Japanese with English abstract).

Ng E (2009). Policies and technical guidelines for urban planning of high-density cities—Air ventilation assessment (AVA) of Hong Kong. *Building and Environment*, 44: 1478–1488.

Oikawa Y (2011). The urban heat island effect in Japan's major cities. *TCC News (Tokyo Climate Center, Japan Meteorological Agency)*, 25: 1–2.

Oke TR (1988). Street design and urban canopy layer climate. *Energy and Buildings*, 11: 103–113.

Omori T, Yang J, Kato S, Murakami S (2003). Radiative heat transfer analysis method for coupled simulation of convection and radiation in large-scale and complicated enclosures, Part 1, accurate radiative heat transfer analysis based on Monte Carlo Method. *Transactions of the Society of Heating, Air-Conditioning and Sanitary Engineers of Japan*, 88: 103–113. (in Japanese)

Ooyama N, Kubota T, Miura M, Mochida A, Tominaga Y (2002). A study on the literature concerning the measurements on a surface temperature in the exterior space: A study on the creation technique and its availability of the living environmental map at a district scale based on a cooperation with self-governing body part 5. In: Summaries of Technical Papers of Annual Meeting Architectural Institute of Japan, D-1: 899–900. (in Japanese)

Pickup J, de Dear RJ (2000). An outdoor thermal comfort index (OUT-SET*)— Part I—The model and its assumptions. In: de Dear R, Kalma J, Oke T, Auliciems A (eds), Turn of the Millennium—Selected Papers from the Conference ICB-ICUC'99, Sydney, Australia, pp. 279–283.

Raisee M, Naeimi H, Alizadeh M, Iacovides H (2009). Prediction of flow and heat transfer through stationary and rotating ribbed ducts using a non-linear k–ε model. *Flow, Turbulence and Combustion*, 82: 121–153.

Richards M, Havenith G (2007). Progress towards the final UTCI model. In: Proceedings of 12th International Conference on Environmental Ergonomics, Ljubljana, Slovenia, pp.521–524.

Sasaki K, Mochida A, Yoshino H, Watanabe H, Yoshida T (2008). A new method to select appropriate countermeasures against heat-island effects according to the regional characteristics of heat balance mechanism. *Journal of Wind Engineering and Industrial Aerodynamics*, 96: 1629–1639.

Sasaki K, Mayer H, Mochida A, Uchida M, Tonouchi T (2009). Field measurement of thermal comfort in outdoor locations—Comparison of SET* and PET based on questionnaire survey. In: Proceedings of 7th International Conference on Urban Climate, Yokohama, Japan.

South China University of Technology (2008). DUTE 1.0 (Design Tool for Urban Residential Area Thermal Environment, Registration number: 2008SR12279).

Spagnolo J, de Dear RJ (2003). A field study of thermal comfort in outdoor and semi-outdoor environments in subtropical Sydney, Australia. *Building and Environment*, 38: 721–738.

Suga K (2003). RANS turbulence modeling for engineering applications. *Journal of Japan Society of Computational Fluid Dynamics*, 11(2): 73–80. (in Japanese)

Suga K (2007). Development of a k–ε model incorporating a cubic eddy-viscosity formulation. *NAGARE (Flow)*, 26: 157–160. (in Japanese)

Tominaga Y, Mochida A, Yoshie R, Kataoka H, Nozu T, Yoshikawa M, Shirasawa T (2008). AIJ guidelines for practical applications of CFD to pedestrian wind environment around buildings. *Journal of Wind Engineering and Industrial Aerodynamics*, 96: 1749–1761.

VDI (2005). Environmental meteorology—Prognostic microscale wind field models—Evaluation for flow around buildings and obstacles, VDI 3783, Part 9.

Wang W-C, Zeng Z, Karl TR (1990). Urban heat islands in China. *Geophysical Research Letters*, 17: 2377–2380.

Yoshida S, Murakami S, Ooka R, Mochida A, Tominaga Y (2000). CFD prediction of thermal comfort in microscale wind climate. In: Proceedings of 3rd International Symposium on Computational Wind Engineering, Birmingham, UK, pp.27–30.

Yahia MW, Johansson E (2013). Influence of urban planning regulations on the microclimate in a hot dry climate: The example of Damascus, Syria. *Journal of Housing and the Built Environment*, 28: 51–65.

Yoshie R, Mochida A, Tominaga Y, Kataoka H, Harimoto K, Nozu T, Shirasawa T (2007). Cooperative project for CFD prediction of pedestrian wind environment in the Architectural Institute of Japan. *Journal of Wind Engineering and Industrial Aerodynamics*, 95: 1551–1578.

Yoshie R, Tanaka H, Shirasawa T (2008). Experimental study on air ventilation in a built-up area with closely-packed high-rise buildings. In: Proceedings of 4th International Conference on Advances in Wind and Structures, Jeju, Korea, pp.1657–1666.